Microscopy and Microanalysis (2021), 1–13
doi:10.1017/S1431927621000064

Microscopy AND Microanalysis

Original Article

Thyroid Gland Alterations in Old-Aged Wistar Rats: A Comprehensive Stereological, Ultrastructural, Hormonal, and Gene Expression Study

Marko Miler[1]*, Vladimir Ajdžanović[1], Jasmina Živanović[1], Jelena Marković Filipović[2], Branka Šošić-Jurjević[1] and Verica Milošević[1]

[1]Department of Cytology, Institute for Biological Research "Siniša Stanković" – National Institute of the Republic of Serbia, University of Belgrade, Belgrade, Serbia and [2]Faculty of Sciences, Department of Biology and Ecology, University of Novi Sad, Novi Sad, Serbia

Abstract

The aim of the present study was to determine and elaborate on all changes in old-aged (OA) versus young-aged (YA) rat thyroids by using stereological, ultrastructural, hormonal, and gene expression analyses. We used 4- and 24-month-old male Wistar rats in our evaluation, presenting all changes in comparison with YA rats. Results showed that the thyroid parenchyma was characterized by higher absolute volumes of the gland, colloid, epithelium, and interstitium by 135, 135, 140, and 142% ($p < 0.05$) respectively, while the relative volumes of colloid and glands were unchanged. Ultrastructural analysis revealed less active glands, with smaller amounts of lysosomes, thyroglobulin (Tg) granules, and microvilli in the luminal colloid. Optical density values for thyroid peroxidase (TPO), Tg, and vascular-endothelial growth factor immunostaining remained unchanged; however, TPO and Tg exhibited visually stronger expression in small active follicles. Thyroxine (T_4)-Tg, the relative intensity of fluorescence (RIF), serum T_4, and the sodium-iodide symporter immunohistochemical and gene expressions decreased by 20, 40, 29, and 31% ($p < 0.05$), respectively, in OA thyroids. Pituitary thyroid-stimulating hormone (TSH) RIF increased by 44% ($p < 0.05$), but the TSH serum concentration remained unchanged. In conclusion, the obtained results indicate depression of the thyroid gland synthetic and secretory capacity with advanced age.

Key words: NIS, T4-Tg, Tg, TPO, TSH

(Received 16 October 2020; revised 15 January 2021; accepted 24 January 2021)

Introduction

Aging is characterized by a progressive loss of physiological integrity at the whole-body level. It leads to a decline in endocrine function inducing somatopause, andropause, and menopause (Chahal & Drake, 2007; Ajdžanović et al., 2018). In humans, the thyroid axis is characterized by normal thyroxine (T_4) and normal or slightly elevated thyroid-stimulating hormone (TSH) levels (Barbesino, 2019). In rats, however, the situation is different, showing normal TSH and lower serum T_4 concentrations with advanced age (Donda & Lemarchand-Beraud, 1989; Silvestri et al., 2008).

Although the first-choice medical examination method for the endocrine system is administering a hormone panel test, in scientific/research examination, valuable data can be obtained from a structural evaluation of endocrine tissues. Structural parameters of the thyroid parenchyma mostly correlate with the activity of the thyroid hormone generating system. Namely, a depleted colloid and higher follicular epithelium suggest an active gland, more precisely, a higher demand for thyroid hormones (TH) and *vice versa*. Reports on Miranda and Sprague–Dawley aging rats showed changes in the thyroid gland relative volume (Mariotti et al., 1995; Moreira et al., 2005); however, data on the respective structural and functional alterations in old Wistar rats is lacking.

Structural analysis on its own is not sufficient to profile the degree of thyroid activity and should be expanded to include a wider morpho-functional characterization of thyroid tissue. We validated a battery of tests using thyroid-specific proteins—thyroid peroxidase (TPO), thyroglobulin (Tg), T_4 bound to Tg (T_4-Tg), and the sodium-iodide symporter (NIS)—which provide valuable additional information on thyroid functioning only from a structural point of view. Namely, the thyroid gland imports iodide, an essential element in TH production, throughout the NIS on the basolateral membrane of the follicular epithelium. Extremely reactive iodide is kept under control by a strong antioxidant defense system in the thyrocyte cytoplasm (Song et al., 2007). Later on, hormone production starts on the border between the follicular epithelial apical membrane and colloid, where TPO localized in the apical membrane (Kotani & Ohtaki, 1987; Fayadat et al., 1998) oxidizes iodide to iodine and incorporates it in the tyrosine residues on Tg (Dunn & Dunn, 2001). TSH stimulation leads both to increased synthesis and secretion of TH.

By an up-to-date screening of the Pubmed database using the keywords thyroid, aging, and rats, we listed only a few papers on structural characteristics, as compared with a huge number of articles dealing with hormonal or molecular biology data (data

***Author for correspondence:** Marko Miler, E-mail: marko.miler@ibiss.bg.ac.rs

Cite this article: Miler M, Ajdžanović V, Živanović J, Marković Filipović J, Šošić-Jurjević B, Milošević V (2021) Thyroid Gland Alterations in Old-Aged Wistar Rats: A Comprehensive Stereological, Ultrastructural, Hormonal, and Gene Expression Study. *Microsc Microanal.* doi:10.1017/S1431927621000064

not shown). Histological analysis is often neglected due to the long period needed for obtaining results, but it represents a valuable tool for identifying structural alterations. Keeping in mind that experiments on aged animals are on the rise, the structural aspect of the study may be a hot topic in current research.

Therefore, we aimed to determine and elaborate all stereological and ultrastructural, as well as hormonal and gene expression data, in the light of establishing a legitimate way to investigate alterations in the old thyroid gland. Our results will help in understanding the thyroid gland structural and functional alterations with advanced age and also provide a novel experimental model that could be adequately exploited and used in further experiments.

Material and Methods

Experimental Animals

The male Wistar rats (4- and 24-month-old) used in the experiment were bred and housed in the Unit for Experimental Animals at the Institute for Biological Research "Siniša Stanković" – National Institute of the Republic of Serbia (IBISS), Belgrade, Serbia. All animals were kept under constant lighting (12 h light–12 h dark) and temperature (21 ± 2°C) conditions and had access to food and water *ad libitum*. All animal procedures were in compliance with the Directive 2010/63/EU on the protection of animals used for experimental and other scientific purposes and were approved by the Ethical Committee for the Use of Laboratory Animals of IBISS, University of Belgrade (No 2-12/12).

Sample Processing

Animals were decapitated without anesthesia, in order to avoid any anesthesia effects on the biochemical and gene expression results. Every effort was made to minimize the suffering of the experimental animals. Blood was collected from the trunk, and a separated serum of all the animals was stored at the same time at −80°C. The animals' pituitary and thyroid glands (one lobe, including part of the trachea) were excised, fixed in 4% paraformaldehyde solution for 24 h, dehydrated in increasing concentrations of ethanol (30–100%) and enlightened in xylene. After embedding in Histowax® (Histolab Product AB, Göteborg, Sweden), each tissue block was serially sectioned at a thickness of 3 μm for pituitaries and 5 μm for thyroids on a rotary microtome (RM 2125RT Leica Microsystems, Wetzlar, Germany). The second thyroid lobe was snap frozen in liquid nitrogen and stored at –80°C for further gene expression analysis. All samples from both YA and OA groups were processed simultaneously.

Histological Analysis

Thyroid sections for the quantitative histological analyses were stained by routine hematoxylin and eosin (H&E) and Masson trichrome staining according to a previously published procedure (Miler et al., 2017; Ajdžanović et al., 2020). Regarding the light microscopy analysis, all digital images of the thyroid sections were made on a LEITZ DM RB Photomicroscope (Leica Mikroskopie & Systems GmbH, Wetzlar, Germany), with a Leica DFC 320 CCD Camera (Leica Microsystems Ltd., Heerbrugg, Switzerland) and LeicaDFC Twain Software (Leica, Germany) for image acquisition and analysis.

Stereological Analysis

Stereological measurements were performed on the H&E-stained thyroid sections, as previously reported by our group (Miler et al., 2014, 2017). In brief, the measurements were carried out using a newCAST stereological software package (VIS—Visiopharm Integrator System, version 3.2.7.0; Visiopharm; Denmark). Total thyroid volumes (mm^3), as well as the total volume of thyroid tissue phases (epithelium, interstitium, and colloid; mm^3), were determined using Cavalieri's principle (Gundersen & Jensen, 1987). Thyroid volume (V_{pt}) is then estimated as

$$\widehat{V}\ pt = a(p) \cdot \mathrm{BA} \cdot \sum_{i=1}^{n} Pi,$$

where $a(p)$ is the area associated with each sampling point (208,878.02 m^2), BA is the block advance representing the mean distance between two consecutively studied sections (150 μm), n is the number of sections studied for each thyroid, and ΣPi is the sum of points hitting a given target (Dorph-Petersen et al., 2001). The same sections were used for the estimation of total thyroid volumes as well as the volumes of thyroid tissue phases: follicular epithelium, interstitium, and colloid. The number of analyzed thyroids was five per group. Volume density estimation was used to determine the percentage of follicular epithelium, interstitium, and colloid. Four to five transversal sections from the anterior, central, and posterior parts of the thyroid ($n = 5$) were analyzed at an objective magnification of ×20. Relative volume densities (V_V) are calculated as the ratio of the number of points hitting each tissue phase divided by the number of points hitting the reference space, that is, analyzed thyroid section: V_V (%) = $Pp/Pt \times 100$ (Pp, counted points hitting the tissue phase, Pt, the total of points of the test system hitting the reference space). Volume density was calculated for each tissue phase per analyzed section. Then, the average value for all analyzed sections was calculated (for each phase separately), representing the relative volume density of the epithelium, interstitium, and colloid. An additional investigator from the field confirmed the findings upon independent analysis.

Ultrastructural Analysis

For the ultrastructural analysis, the thyroid lobe was removed from two animals per group and processed as previously described (Živanović et al., 2019). The thyroid lobe was sliced in 4% glutaraldehyde solution in 100 mM phosphate buffer, pH 7.4, for 24 h. Postfixation was carried with 1% OsO4 for 1 h at 4 °C, and counterstaining with uranyl acetate. Samples were dehydrated through a graded series of ethanol and embedded in Araldite resin. A Leica EM UC7 ultramicrotome (Leica, Germany) with a Diatome ultra 45° diamond knife (Diatome, Switzerland) was used for cutting ultrathin sections of thyroid tissue at a thickness of 70 nm. Grids with ultrathin sections were stained with uranyl acetate and lead citrate and examined under a Morgagni 268 (FEI Company, Eindhoven, The Netherlands) transmission electron microscope.

Immunohistochemistry and Immunofluorescence

Representative thyroids sections were immunohistochemically (IHC) stained, while representative pituitary and the remaining thyroid sections were immunofluorescently (IF) stained according

Table 1. List of Antibodies Used in Immunohistochemical (IHC) and Immunofluorescent (IF) Analysis.

	Name	Cat. Number	Origin	Dilution	Manufacturer
Primary antibodies used					
IHC	TPO	sc-376876	Mouse	1:400	Santa Cruz, Italy
	Tg	A0251	Rabbit	1:500	Dako, Denmark
	NIS	EUD4101	Rabbit	1:1,200	Acris, Germany
	VEGF	ab46154	Rabbit	1:100	Abcam, UK
IF	TSH	AFP-1274789	Rabbit	1:1,000	Bethesda, MD, USA
	T_4-Tg	12102	Mouse	1:300	Bioscience, USA
Secondary antibodies used					
IHC	Anti-mouse, HRP labeled	Ab6820	Donkey	1:100	Abcam, UK
	Anti-rabbit, HRP labeled	P0399	Swine	1:100	Dako, Denmark
IF	Anti-mouse, Alexa Fluor 488	A-21202	Donkey	1:500	Thermofisher, CA, USA

to previously described procedures (Miler et al., 2014, 2017, 2020; Šošić-Jurjević et al., 2015).

Immunohistochemical Analysis

After tissue deparaffinization, endogenous peroxidase activity was blocked by incubation of sections with 0.3% hydrogen peroxide in methanol for 15 min. Then, thyroid sections were exposed to heat-induced antigen retrieval to unmask target antigens. Slides were placed in a container, covered with 100 mM sodium citrate buffer (pH 6.0), and heated at 750 W in a microwave oven for 10 and 5 min, respectively. The reduction of nonspecific background staining was achieved by incubation with normal porcine serum (Dakopatts, Glostrup, Denmark) diluted 1:10 for 45 min.

For a functional IHC analysis, the antisera directed against TPO, Tg, NIS, and vascular-endothelial growth factor (VEGF) were applied overnight at 4°C. For the negative control thyroid sections, the primary antibody was substituted with phosphate-buffered saline (PBS).

For the immunodetection of TPO, Tg, NIS, and VEGF proteins, secondary antibodies (HRP labeled) were applied for 1 h. Visualization was performed using the Dako liquid diaminobenzidine tetrahydrochloride substrate chromogen system (Dako North America, Inc. Carpinteria, CA, USA) at concentrations suggested by the manufacturer. All washes and dilutions were done using 100 mM PBS pH 7.4. Hematoxylin was used as counterstain and slides were mounted in a DPX medium (Sigma-Aldrich, Barcelona, Spain).

Immunofluorescent Analysis

For the IF analysis of pituitary and thyroid sections, the reduction of nonspecific background staining was achieved by incubation with normal donkey serum (Abcam, Cambridge, MA, USA), diluted 1:10 for 30 min. Primary anti-TSHβ antibody was applied on pituitary sections overnight at room temperature (RT). Secondary antibody Alexa Fluor 488 was applied for 1 h at RT. The list of used antibodies is shown in Table 1. The sections were then washed in PBS with 0.1% Tween 20 five times for 5 min and coverslipped with Mowiol 4–88 (Sigma-Aldrich Co., St. Louis, MO, USA). Images were obtained using a confocal laser scanning microscope Leica TCS SP5 II Basic (Leica Microsystems CMS GmbH; Germany). An Ar-ion 488-nm laser was used for excitation of fluorescence.

The rabbit antisera, directed against human T_4 bound to thyroglobulin, were applied overnight at 4°C. Alexa Fluor 488 was applied as a secondary antibody. The sections were subsequently washed in PBS five times for 5 min. Afterward, the sections were incubated with RNase A (10 μg/mL; Thermo Fisher Scientific Inc., Rockford, IL, USA) for 20 min at 37°C, and the nuclei were counterstained with propidium iodide (diluted in 2× saline sodium citrate buffer, SSC, 1:300) for 1.5 min. Sections were washed three times for 1 min in 2× SSC buffer and one time for 5 min in PBS and coverslipped with Mowiol 4–88 (Sigma-AldrichCo., St. Louis, MO, USA). Images were obtained using a confocal laser scanning microscope Olympus FV10-ASW (Olympus FLUOVIEWFV1000; Germany). Ar-ion (488 nm) and HeNe (543 nm) lasers were used for excitation of fluorescence.

Quantitative Image Analysis

Quantification of IHC Signal

The stained percentage color area for the DAB immunopositive follicles of TPO, Tg, and VEGF was evaluated using a Windows based ImageJ (Image J, Version 1.49j) plugin named the IHC profiler according to previously described procedures (Ajdžanović et al., 2016; Miler et al., 2017). For the analysis of DAB immunopositive follicles, 10 randomly captured images (the Leica light microscopic tool has already been described; 2088 × 1550 pixels, ×10 objective magnification) per thyroid tissue per animal were analyzed.

Quantification of IF Signal

The analysis of TSH RIF signal was performed as previously reported by our group (Miler et al., 2020). An analysis of confocal microscopy images was done using the quantify option in the LAS AF Lite software (Leica Application Suite Advanced Fluorescence Lite/1.7.0 build 1240, Leica Microsystems CMS GmbH; Germany).

The regions of interest were encircled with freeform drawing tools and included the intense spots of the TSHβ-immunopositive granules within the cytoplasm of pituitary thyrotrophs. Two different immunonegative spots outside of the TSHβ-immunopositive thyrotrophs served as referent particles for the definition of background fluorescence. The mean of the two measurements was calculated and then used for relative intensity of fluorescence (RIF) determination. To calculate the RIF, the determined average of mean value was

subtracted from the average of background fluorescence. The intensity of fluorescence was determined in 200 pituitary thyrotrophs per animal, and in three animals per group in which the cell nuclei were apparent.

The measurement of T_4-Tg RIF was achieved using the ImageJ software (Image J, Version 1.49j) according to our previous work (Šošić-Jurjević et al., 2014; Miler et al., 2017). In brief, thyroid T_4-Tg IF-stained follicles were encircled with a freeform drawing tool, measuring the integrated density (ID) of 50 immunopositive follicles per thyroid tissue per animal. Three other immunonegative spots in proximity to the IF-stained follicles were also rounded for the measurement of the mean fluorescence of background readings (MB). RIF was calculated using the formula: RIF = ID − (CA × MB), where CA represents the area of selected follicles.

Quantification of NIS Relative Volume Density

The relative volume density of the NIS-immunopositive epithelium was quantified at 10× magnification with a 4 × 4 generated grid. V_V NIS-immunopositive epithelium was defined as the relative ratio of the sum of hits falling on the basolateral membrane and cytoplasm and the sum of hits falling on the epithelium, interstitium, and colloid, that is, the relative volume of the thyroid glands. Values are multiplied by 100 and expressed as percentages (%).

Hormonal Analysis

The serum was separated from trunk blood after decapitation and left at room temperature for 2 h, after which it was stored at −70°C. The serum levels of TSH and total T_4 were measured by enzyme-linked immunosorbent assay (ELISA) using a rat TSH kit (IBL International GmbH, Hamburg, Germany) and a T_4 kit provided by Cusabio Biotech Co. Ltd (Wuhan, Hubei, China). All samples were assayed in duplicate together in one run with an intra-assay coefficient of variation of 8.8% (measuring range 10–320 ng/mL) for TSH and < 15% (measuring range 0.85–3.23 ng/mL) for T_4.

RNA Isolation, cDNA Transcription, and Real-Time PCR

A total RNA from thyroids was isolated using TRIzol (Invitrogen, Carlsbad, CA) and further purified using the RNeasy mini-kit (QIAGEN, Hilden, Germany) following the manufacturer's instructions. cDNA was synthesized using the High Capacity cDNA Reverse Transcription Kit (Applied Biosystems, Vilnius, Lithuania) with 500 ng of RNA. PCR amplifications of cDNAs were performed in a real-time PCR machine ABI Prism 7000 (Applied Biosystems, USA) with SYBRGreen PCR master mix (Applied Biosystems, USA). The program included the following conditions: 3 min at 95°C, followed by 40 cycles of 15 s at 95°C, 30 s at 60°C, and 30 s at 72°C. The list of primers used is shown in Table 2. Melting curve analysis was used to confirm gene-specific amplification. Nuclease-free water was used as negative control instead of the cDNA template. The expression level of each gene was calculated using the formula $2^{-(\Delta\Delta Ctexp-\Delta\Delta Ctcontrol)}$, where ΔCt is the difference between the cycle threshold value of the gene of interest and the cycle threshold value of *Gapdh* as a reference gene. All the data were calculated from duplicate reactions. RNA data are presented as average relative levels versus *Gapdh* ± SD.

Table 2. List of Primers Used in Real-Time PCR Analysis.

Gene	Primer Sequence
Tpo	f: 5′-TTGGATCTGGCATCACTGAACTT-3′ r: 5′-ATCTTGTTGACCATGCTTCTGTTG-3′
Tg	f: 5′-CCGGATATTGCAGAGACGAT-3′ r: 5′-GGCAGCTTGGGATATATGGA-3′
Nis	f: 5′-GGTGTCATCAGTGGGCCTCTA-3′ r: 5′-CCCGTGTCCATTCCAGAACTG-3′
Sod1	f: 5′-AAGCGGTGAACCAGTTGTG-3′ r: 5′-CCAGGTCTCCAACATGCC-3′
Sod2	f: 5′-GGTGGAGAACCCAAAGGAGA-3′ r: 5′-AGCAGTGGAATAAGGCCTGT-3′
Cat	f: 5′-CCAGCGACCAGATGAAGCA-3′ r: 5′-TGGTCAGGACATCGGGTTTC-3′
Gpx	f: 5′-TATAGAAGCCCTGCTGTCCA-3′ r: 5′-CAAGCCCAGATACCAGGAA-3′
Gr	f: 5′-ACGAGGAAGACGAAATGCGTGATG-3′ r: 5′-AGGATGAATGGCGA CGCTATTGTC-3′
Nrf2	f: 5′-GAGCGGGAGAAATCACACAGAATG-3′ r: 5′-CAGGAGCTGCATGCACTCATCG-3′
Gapdh	f: 5′-GTGGACCTCATGGCCTACAT-3′ r: 5′-GGATGGAATTGTGAGGGAGA-3′

Table 3. Absolute Mass and Relative Weight of Thyroid in Young (YA) and old Animals (OA).

Groups	Body Mass (g)	Absolute Thyroid Weight (mg)	Relative Thyroid Weight (mg x 100/ b.m.)
YA	470 ± 39	11.3 ± 1.3	2.2 ± 0.2
OA	697 ± 45	20.2 ± 3.1	2.6 ± 0.6

Results are expressed as means ± SD, $n = 6$.

Statistical Analyses

Statistical analyses of all the obtained results were performed using GraphPad Prism v.6 for Windows (San Diego, CA, USA). The data for the experimental groups were first tested for normality of distribution with the Kolmogorov–Smirnov test. After the confirmation of Gaussian distribution and the homogeneity of variance with Bartlett's test, unpaired Student's *t*-test was used to evaluate differences between the groups. A confidence level of $p < 0.05$ was considered statistically significant. The data are presented as means ± SD.

Results

Body Mass and Absolute and Relative Thyroid Weight

Body mass and absolute thyroid weight expectedly increased in OA group by 47 and 78% ($p < 0.05$; Table 3) respectively, in comparison with YA, while the relative thyroid weight remained unchanged (Table 3).

Histological and Stereological Results

The thyroid parenchyma of both YA and OA groups were characterized by variability in the size of follicles and the

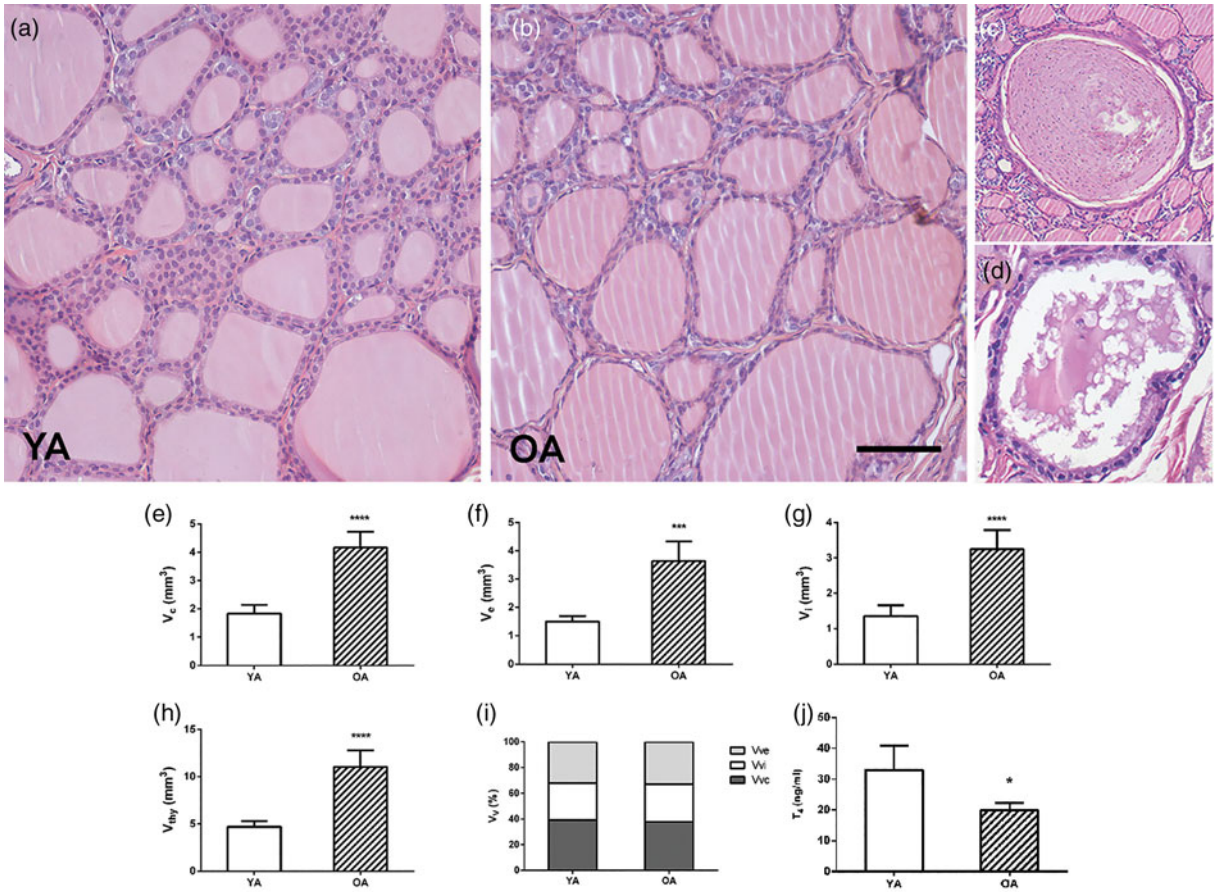

Fig. 1. Representative micrographs of hematoxylin and eosin-stained thyroid sections of (**a**) young- (YA) and (**b**) old-aged (OA) male Wistar rats. 20× magnification, bar = 50 μm. Representative micrographs of atrophic cysts: (**c**) follicular and (**d**) ultimobranchial. Absolute volume densities (V, mm^3) of (**e**) epithelium, (**f**) interstitium, (**g**) colloid, and (**h**) thyroid gland. (**i**) Relative volume density (Vv; %) of thyroid phases. All the values are presented as mean ± SD (n = 5); statistics: Student's t-test, $^*p < 0.05$. (**j**) Serum level of T_4 (ng/mL). All the values are presented as mean ± SD (n = 6); statistics: Student's t-test, $^*p < 0.05$.

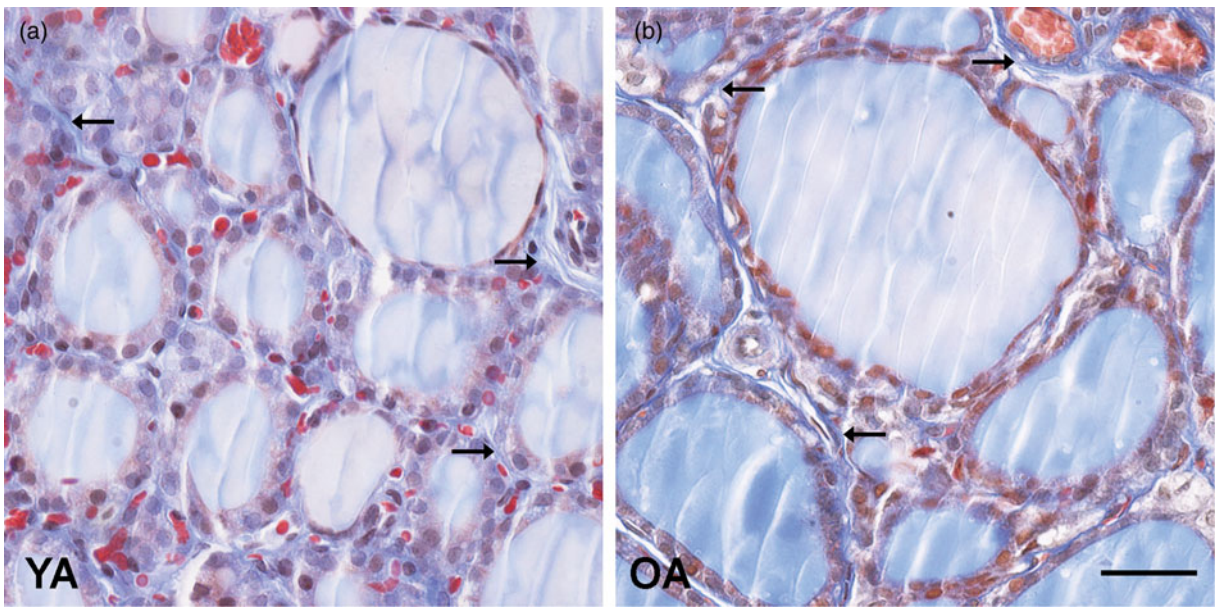

Fig. 2. Representative micrographs of Masson trichromatic-stained thyroid sections of (**a**) young- (YA) and (**b**) old-aged (OA) male Wistar rats. Arrows show collagen fibers. 40× magnification, bar = 25 μm.

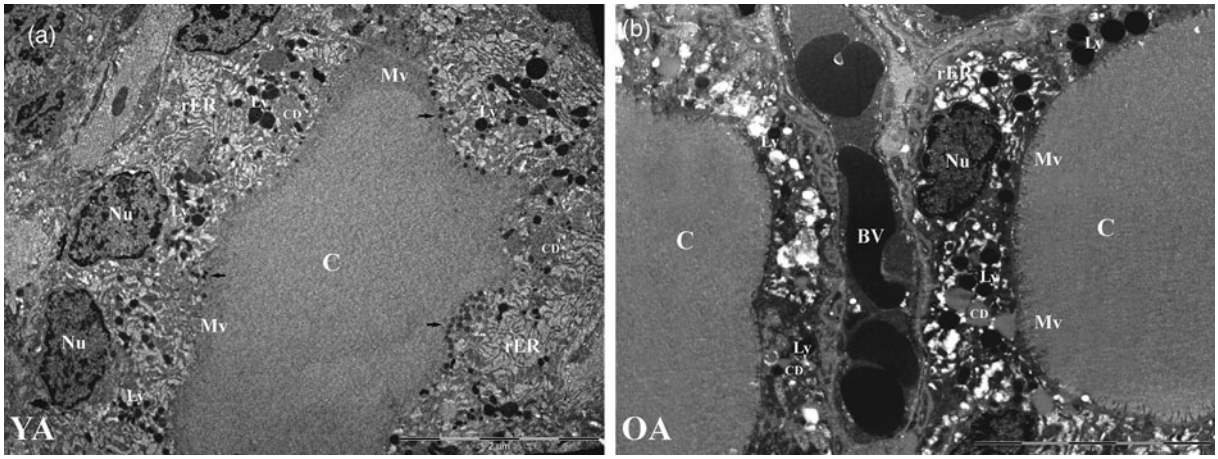

Fig. 3. Representative ultramicrographs of (**a**) young- (YA; 2800× magnification) and (**b**) old-aged (OA; 3500× magnification) male Wistar rats. Nu, nucleus; Ly, lysosomes; rER, rough endoplasmic reticulum; C, colloid; CD, colloid droplets; Mv, microvilli; arrows, Tg granules.

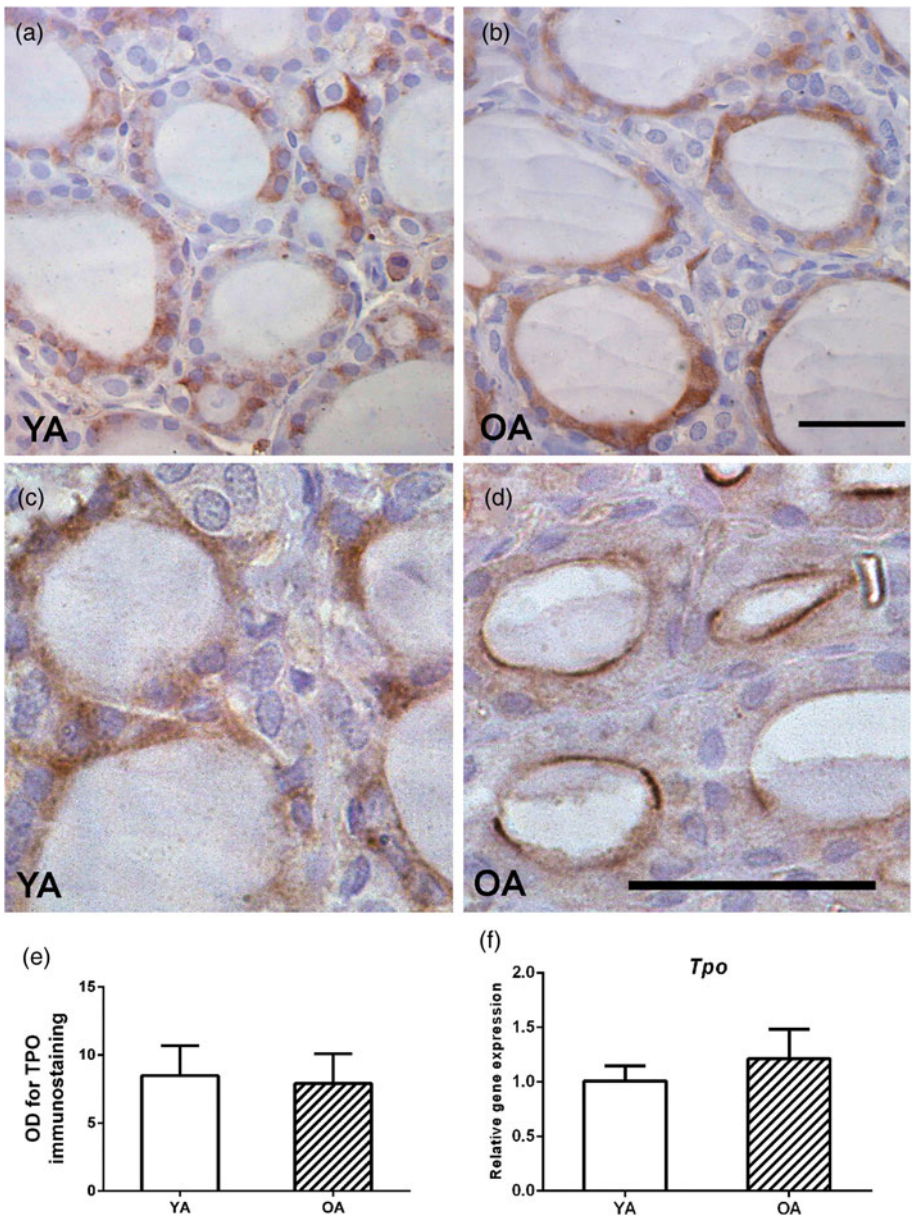

Fig. 4. Representative micrographs of TPO IHC expression in thyroids of (**a**) young- (YA) and (**b**) old-aged (OA) male Wistar rats. 40× magnification, bar = 25 μm. Small follicles of (**c**) YA and (**d**) OA thyroids. (**e**) TPO optical density (OD), each value represents mean ± SD, n = 4. (**f**) Relative mRNA level of *Tpo*, each value represents mean ± SD, n = 6; statistics: Student's t-test.

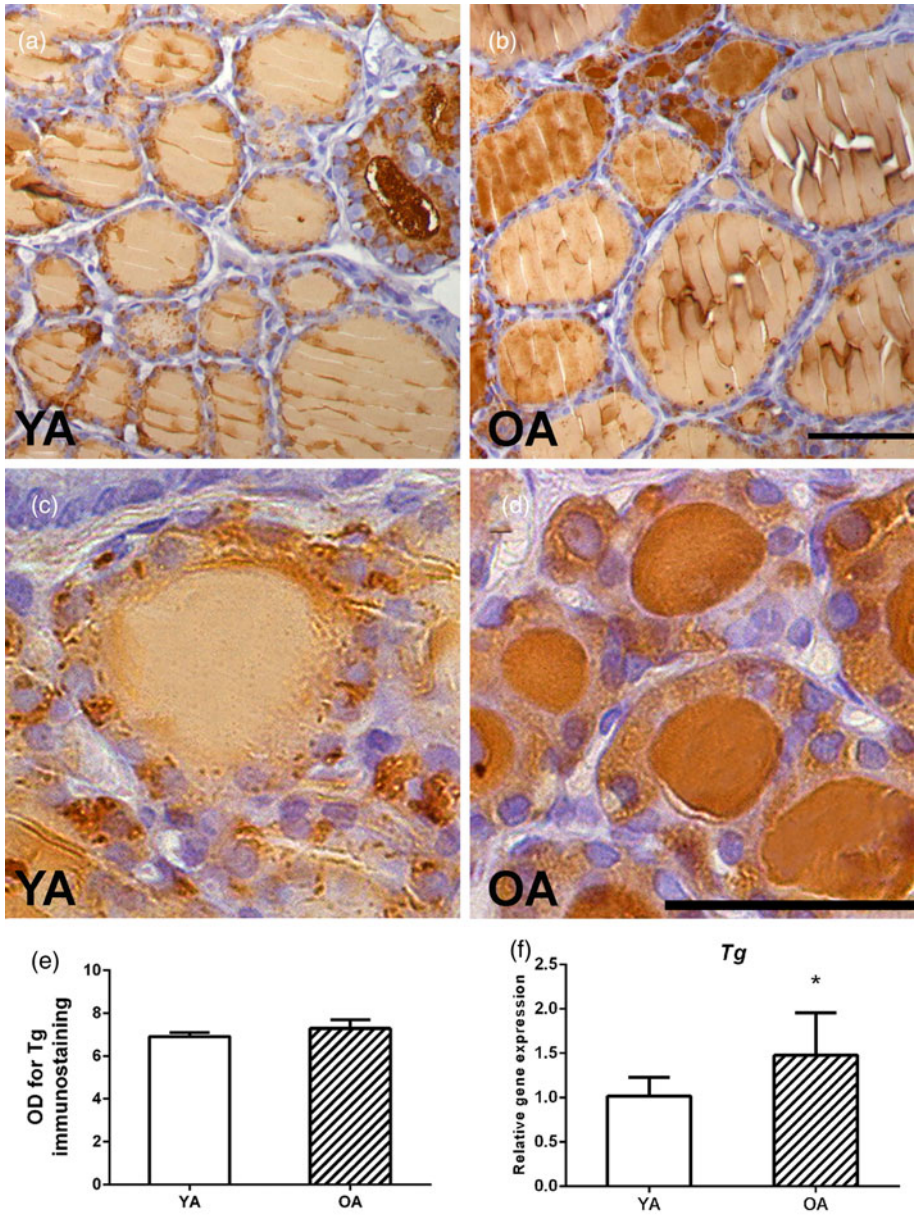

Fig. 5. Representative micrographs of Tg IHC expression in thyroids of (**a**) young- (YA) and (**b**) old-aged (OA) male Wistar rats. 40× magnification, bar = 25 μm. Small follicles of (**c**) YA and (**d**) OA thyroids. (**e**) Tg optical density (OD), each value represents mean ± SD, $n = 4$. (**f**) Relative mRNA level of *Tg*, each value represents mean ± SD, $n = 6$; statistics: Student's *t*-test, $^*p < 0.05$.

amount of luminal colloid (Figs. 1a, 1b). Bigger follicles composed of a flattened follicular epithelium and a distended colloidal lumen were more numerous in comparison with smaller, more active ones (Figs. 1a, 1b). Collagen connective tissue in the interstitium of OA thyroids was represented like in the YA group (Fig. 2). The presence of atrophic cysts, both follicular (Fig. 1c) and keratinized (Fig. 1d), was noted in the OA thyroids.

Stereological analysis demonstrated that the absolute volume of the thyroid gland, colloid, interstitium, and epithelium in the OA group increased by 135, 135, 140, and 142% ($p < 0.05$; Figs. 1e–1h) respectively, in comparison with the values obtained for YA. However, the relative volume density of the colloid, interstitium, and epithelium remained unchanged in comparison to the young controls (Fig. 1i).

Ultrastructural Analysis

The thyrocytes of the thyroid gland of YA rats show a regular structure with basal-apical orientation. The euchromatin nucleus (Nu) positioned basally is surrounded by a developed, dilated rER network (Fig. 3a). A large number of polymorphic lysosomes (Ly) is found in the cytoplasm, with colloidal droplets (CDs) of different diameters (Fig. 3a). The cuboidal epithelium indicates a very dynamic and active gland, both in terms of thyroglobin synthesis (arrows in Fig. 3a) and the process of its breakdown (colloidal drops surrounded by lysosomes; Fig. 3a). In the thyrocytes of the thyroid gland of OA rats, the polarization of the cell from the basal to the apical pole is preserved. The nucleus (Nu) is localized basally and dilated rER cisterns are observed around it (Fig. 3b). The follicular epithelium is low-prismatic. At the apical

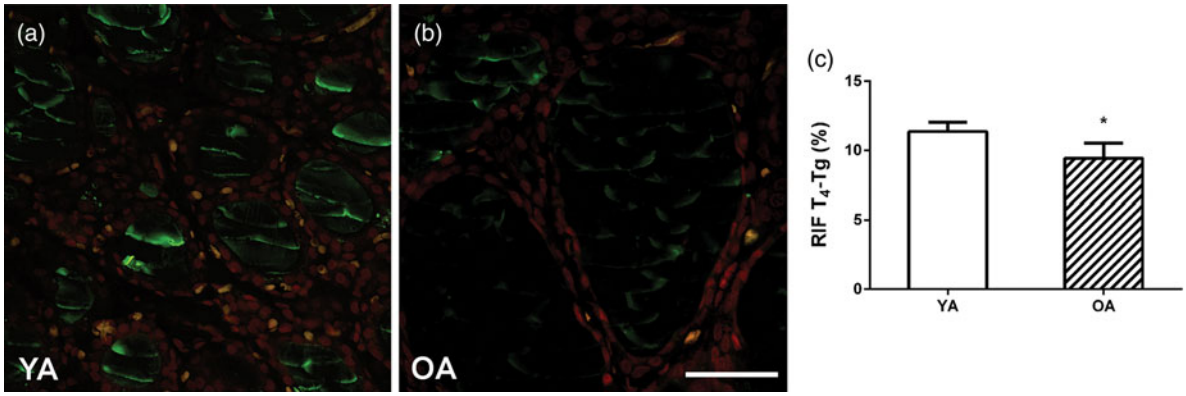

Fig. 6. Representative micrographs of T_4-Tg IF signal in thyroids of (**a**) young- (YA) and (**b**) old-aged (OA) male Wistar rats. 40× magnification, bar = 25 μm. (**c**) Relative intensity of fluorescence (RIF) of T_4-Tg, each value represents mean ± SD, $n = 4$. Student's t-test, $^*p < 0.05$. Green signal represents T_4-Tg, whereas red signal represents nuclei.

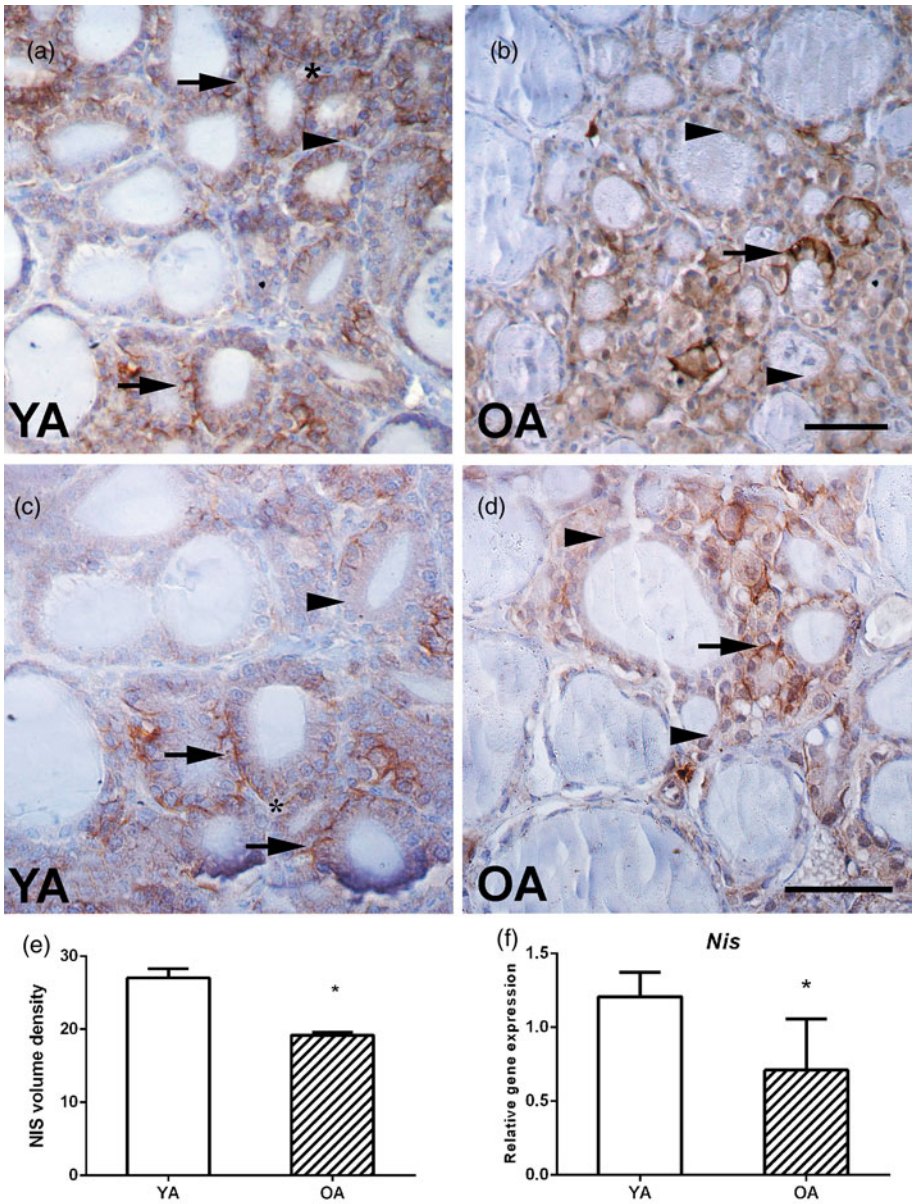

Fig. 7. Representative micrographs of NIS IHC expression in thyroids of (**a**, **c**) young- (YA) and (**b**, **d**) old-aged (OA) male Wistar rats. 20× and 40× magnification, bar = 50 and 25 μm, respectively. Arrows—NIS basolateral expression; arrowhead—NIS cytoplasmic expression; asterisk—regions of NIS expression. (**e**) Relative volume density of NIS, each value represents mean ± SD, $n = 4$. (**f**) Relative mRNA level of *Nis*, each value represents mean ± SD, $n = 6$; statistics: Student's t-test, $^*p < 0.05$.

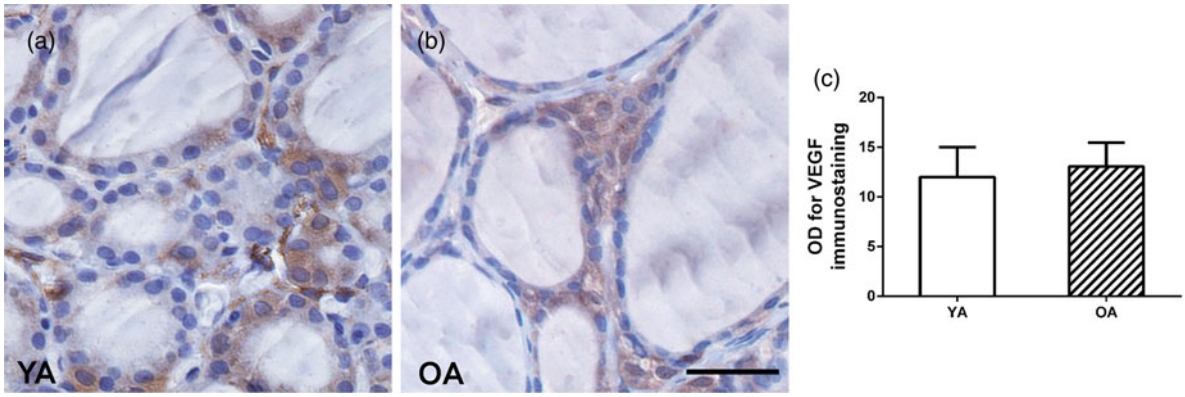

Fig. 8. Representative micrographs of VEGF IHC expression in thyroids of (**a**) young- (YA) and (**b**) old-aged (OA) male Wistar rats. (**c**) VEGF optical density (OD), each value represents mean ± SD, $n = 4$; statistics: Student's t-test. 40× magnification, bar = 25 μm.

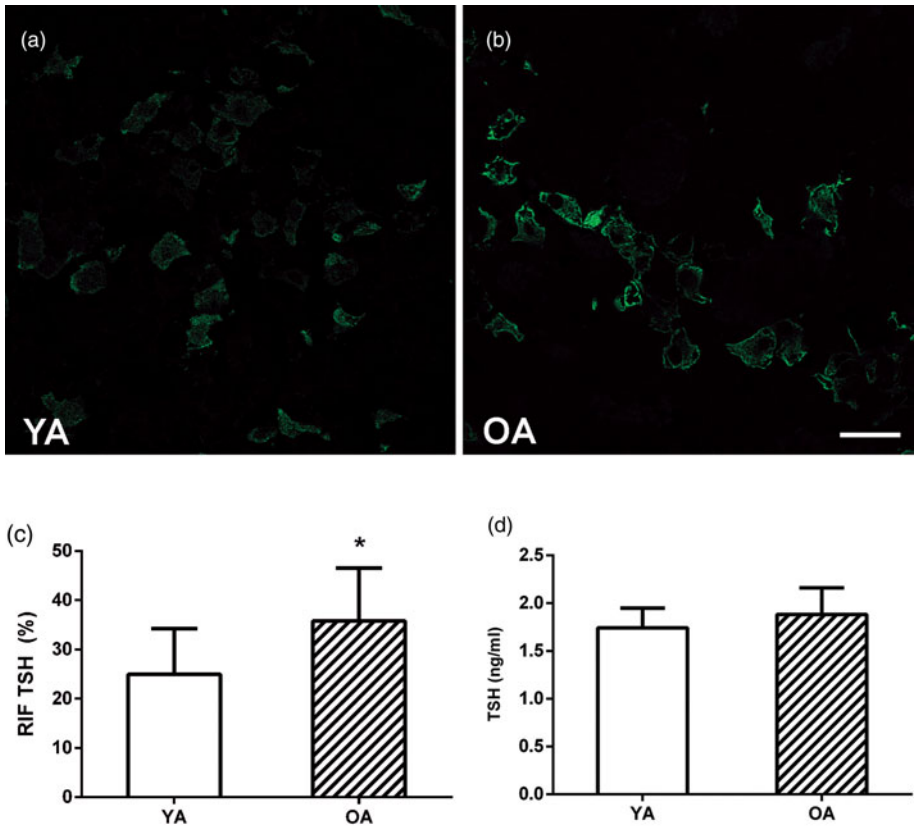

Fig. 9. Representative micrographs of TSH IF signal in pituitaries of (**a**) young- (YA) and (**b**) old-aged (OA) male Wistar rats. 40× magnification, bar = 25 μm. (**c**) Relative intensity of fluorescence (RIF) of TSH. Green signal represents TSH granules. (**d**) Serum level of TSH (ng/mL). All the values are presented as mean ± SD ($n = 6$); statistics: Student's t-test, $^*p < 0.05$.

membrane, much lesser microvilli (Mv) were immersed in the lumen of the colloid when compared with YA thyrocytes (Fig. 3b). Besides colloid droplets, cytoplasm contains lysosomes (Ly) of different sizes, as well as small, dark vesicles near the apical pole, carrying newly synthesized thyroglobulin (arrow in Fig. 3b), however, both less numerous than in the YA group.

Morpho-Functional Characterization of the Thyroid

In comparison with YA, in the OA thyroids, there is no difference in TPO expression (Figs. 4a, 4b, 4e). In both groups, the heterogeneity of TPO expression is noticed between follicles, and also within one follicle, so some thyrocytes show a strong TPO signal, while in others, there is no TPO signal (closer insight in Figs. 4c, 4d). TPO localization is apical and cytoplasmic, while some small thyrocytes in the OA group have pronounced apical localization (Figs. 4c, 4d).

An analysis of Tg expression showed an intensive granular signal in the cytoplasm of the follicular epithelium and a weak Tg signal in most of the YA follicles (Figs. 5a, 5c). Small follicles are occasionally observed, characterized by an intense Tg signal in the luminal colloid of OA follicles (Fig. 5b). Darker, more

intensely colored small follicles in the parenchyma of the OA rat are more numerous, although a stronger granular cytoplasmic signal is present in the YA group (closer insight in Figs. 5c, 5d). The optical density of Tg immunostaining remained unchanged between the two examined groups (Fig. 5e).

The IF expression of T_4 bound to Tg was characteristic of the follicles in the central part of the thyroid gland of YA rats, with a strong IF signal in the part of the colloid adjacent to the apical membrane of the thyrocytes (Fig. 6a). In the OA, the central region follicles of larger dimensions are characterized by a lacking or weak IF signal in the luminal colloid (Fig. 6b). Quantitative IF analysis showed 20% ($p < 0.05$) decreased RIF in the OA group in comparison with the values of the YA group (Fig. 6c).

In the YA group, intensely stained follicles are scattered and form regions of NIS expression within the tissue of the thyroid gland (asterisk in Figs. 7a, 7c), which are more prevalent in this group than in OA animals (Figs. 7b, 7d). In both YA and OA animals, a strong signal was observed only on the basolateral membrane of small-sized follicles (arrow in Fig. 7). In larger-sized follicles, the NIS signal is present only in the cytoplasm or is absent (arrowhead in Fig. 7). Quantitative analysis of the thyroid gland showed that the volume density of NIS positive follicles in the YA group was 29% higher ($p < 0.05$) in comparison with the value obtained for the OA group (Fig. 7e).

The intensity of VEGF signal varies between follicles (Fig. 8). The heterogeneity of the intensity of VEGF signal is observed even among the thyrocytes of the same follicle (Fig. 8). IHC VEGF signal in the thyroid gland of OA rats is present only in the follicular epithelium of smaller, more active follicles, whereas in the large, inactive ones it is partially absent (Fig. 8a).

Pituitary TSH Cells Evaluation

The pituitary TSH IF signal was located in the cytoplasm of thyrotrophs of both experimental groups (Figs. 9a, 9b), whereas vacuoles were observed only in the OA group (Fig. 9b). Young male rats' pituitary thyrotrophs (Fig. 9a) had lesser amounts of TSH within their cytoplasm in comparison with the old ones (Fig. 9b). The intensity of the TSH RIF signal was lower by 44% ($p < 0.05$; Fig. 9c) in comparison with the OA value.

Hormonal Analysis

Serum T_4 concentration in the OA group was 40% lower ($p < 0.05$; Fig. 1j) in comparison with the values obtained for YA. The TSH level remained unchanged (Fig. 9d).

qPCR Analysis

Our gene expression analysis showed that OA was characterized by higher mRNA levels of *Tg*, *Sod1,* and *Cat* by 45, 113, and 136% ($p < 0.05$; Fig. 5f; Supplementary Figs. S1A, S1C), respectively, while the mRNA level of *Nis* decreased by 31% ($p < 0.05$; Fig. 7f), all in comparison with the YA group. The gene expressions of *Tpo*, *Sod2*, *Gpx*, *Gr,* and *Nrf2* (Fig. 4f; Supplementary Figs. S1B, S1D, S1E, S1F) remained unchanged.

Discussion

The present study aimed to report and evaluate all alterations in the thyroid glands of old-aged male Wistar rats, with a focus on stereological, ultrastructural, hormonal, and gene expression analyses. We identified changes that included an increment in the absolute thyroid volume, bigger inactive follicles, stronger TPO and Tg expression in smaller active follicles, downregulation of NIS IHC and gene expressions, upregulation of *Tg*, *Cat,* and *Sod1*, lower capacity to produce T_4, a lower serum T_4 level, and an increase in pituitary TSH RIF, all in comparison with YA rats. Overall, the obtained results indicate depression of the thyroid gland synthetic and secretory capacity with advanced age.

After performing an unbiased stereological analysis, we concluded that the OA thyroid glands were characterized by an increment in the total gland and individual phases' absolute volume. Follicles in the OA group were bigger in diameter and size, dilated, with flattened epithelium, suggesting an inactive thyroid state, while the presence of smaller follicles was noticed to a lesser extent. Aging has been reported to cause a decrement in relative follicular epithelium and an increase in colloid volume in Miranda and Spague–Dawley rats (Mariotti et al., 1995; Moreira et al., 2005); however, we report that the relative thyroid volume remained unchanged. Sometimes, an increase or decrease in the size, volume, or mass of an organ suggests overstimulation or inhibition of the thyroid gland (Šošić-Jurjević et al., 2014; Giuliani et al., 2017), but this result was anticipated in our study because Wistar rats grow throughout their lives (Rao-Rupanagudi et al., 1992).

Further evaluation of the OA thyroid parenchyma showed the presence of cystic atrophy, namely cysts that were lined by flattened or ciliated epithelium (follicular cysts) or filled with keratinized material (ultimobranchial cysts). The presence of cysts is a characteristic sign of an inactive gland, and this is in accordance with the observation of Martin-Lacave et al. (1992); however, unlike in their results, connective tissue (collagen) did not increase in comparison with the YA group. In addition, our results show no inflammatory reaction or accumulation of lipid droplets in the thyroid parenchyma, which is in line with some already published data (Rao-Rupanagudi et al., 1992; Lee et al., 2016).

Results obtained by TEM revealed that OA thyroids have lower secretory activity which is characterized by reduced lysosomes and Tg granules in the thyrocyte cytoplasm and lesser microvilli in the thyroid lumen. Such an ultrastructural milieu is in line with the decrement of thyroid capacity to respond to TSH, since the lysosome number immediately increases in response to TSH (Uchiyama et al., 1986). Even the unchanged TSH level in OA rats is in line with the results of Donda & Lemarchand-Beraud (1989), as the number of TSH receptors (TSHR) on the thyrocyte surface decrease with advanced age (Armengol et al., 2001), leading to a depression of T_4 secretion. Moreover, even though the TSH RIF signal shows TSH granule accumulation in the thyrotrophs, lower T_4 was not a sufficient stimulus for a positive feedback loop response, suggesting central deregulation of this axis with advanced age.

The functional characterization of thyroid specific proteins (TPO, Tg, T_4-Tg, and NIS) was used as a powerful tool in the morpho-functional evaluation of the thyroid gland. Herein, we showed that the TPO IHC expression pattern remained unchanged with advanced age. This was followed by an unaltered *Tpo* mRNA level in the OA group, despite the fact that *Tpo* gene expression was shown to decrease in old Dutch–Miranda male rats (Corrêa Da Costa et al., 2001). Interestingly, we observed intensive TPO apical localization in some small OA follicles; of note, only the apical localization of TPO is responsible for TH synthesis (Kotani & Ohtaki, 1987; Fayadat et al., 1998). In

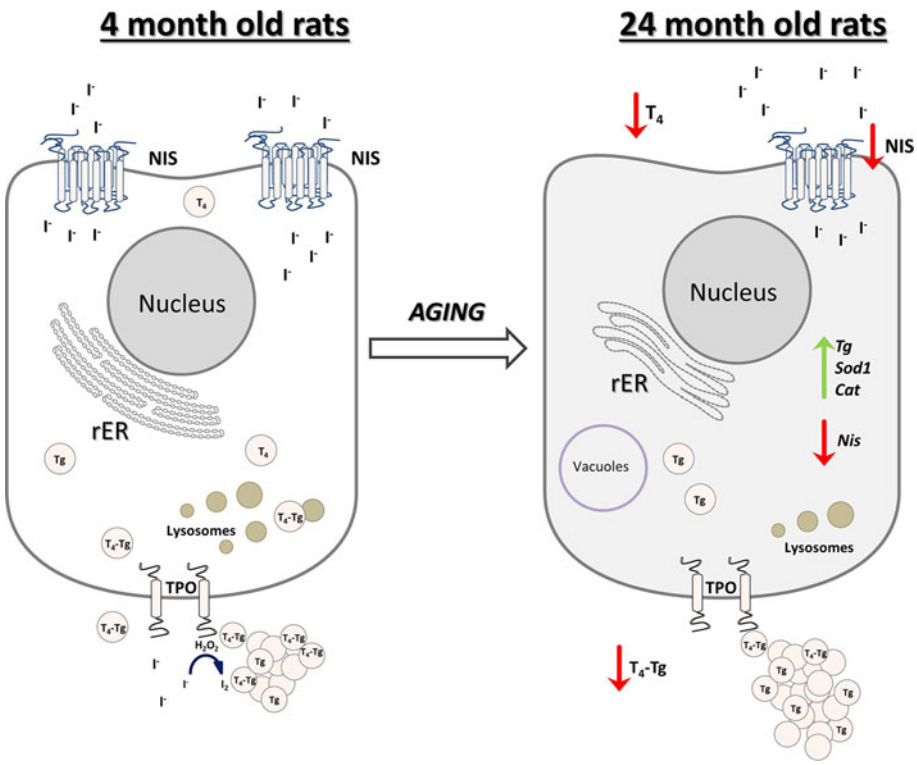

Fig. 10. Schematic representation of thyroid gland structural and functional alterations during aging in male Wistar rats. Old-aged thyroids are characterized by lower NIS expression thus lower iodide import. Dilated rER and a smaller number of lysosomes indicate decreased synthesis and secretion of T_4, which leads to lower T_4 concentration in serum of old-aged rats. *Cat*, catalase; H_2O_2, hydrogen peroxide; I^-, iodide; I_2, iodine; NIS, sodium iodide symporter; rER, rough endoplasmic reticulum; T_4, thyroxine; Tg, thyroglobulin; T_4-Tg, T_4 bound to Tg; TPO, thyroid peroxidase; *Sod1*, superoxide dismutase 1.

addition, TSH is a controller of TPO expression, while antibodies to TPO arise spontaneously with age (Chen et al., 2010), leading to interference with TH production.

In line with TPO, we noticed stronger Tg expression, yet again, in small OA follicles. Tg is localized in the thyroid colloid where it serves as a depot for TH. Average Tg OD did not differ between the examined groups, but the stronger Tg IHC expression in small follicles was in accordance with the upregulation of *Tg* mRNA transcription, suggesting Tg accumulation in the OA colloid. Our findings differ from the results obtained in Dutch–Miranda old rats, showing a decrement in *Tg* mRNA level by 50% (Corrêa Da Costa et al., 2001). The obtained difference in *Tpo* and *Tg* mRNA levels is obviously a consequence of different rat strains used in the evaluations.

Nevertheless, we noticed a decrement in the T_4-Tg IF signal intensity in the OA group. The T_4-Tg antibody is a marker of newly synthetized T_4 in the thyroid luminal colloid (Faggiano et al., 2004) and its decrease emphasizes lower T_4 production. Although Tg accumulates in some small follicles, it is not iodized, leading to T_4 depletion, which was followed by lower T_4 serum concentrations in old animals. These results suggest the thyroid gland's capacity to produce and accumulate Tg in small, active follicles. However, there is a decrement in T_4 production, which is not sufficient to cause a change in the circulating T_4 level.

In addition, we measured the NIS relative volume density, as NIS transport iodide, an inevitable element of TH synthesis (Bizhanova & Kopp, 2009). We determined that the basolateral membrane of OA thyroids showed significantly lower expression of NIS, which is in accordance with the lower *Nis* mRNA level (Faggiano et al., 2004). Physiologically speaking, the more abundant NIS expression in YA rats provides higher iodide import from circulation, thus more TH production and *vice versa*. The downregulation of NIS expression is in line with lower ability of the gland to respond to TSH.

Since the uptake of highly reactive iodide is decreased; however, this result supports the preserved antioxidant defense in the OA thyroid. Nrf2 is activated in an environment with iodide surplus to prevent damage to proteins and DNA which would be detrimental in OA thyroids (Wang et al., 2017). Conversely, we reported upregulation of *Cat* and *Sod1* gene transcription in OA thyroids, suggesting that this alteration is clearly a result of the aging process, especially since the *Nrf2* mRNA level remained unchanged in OA thyroids.

Lastly, we analyzed the expression of VEGF, an angiogenic factor and a key player in the process of new blood vessel formation. Our results revealed that the VEGF IHC signal manifested the same expression pattern in both experimental groups. Increasing vascularity surrounding thyroid follicles may also promote cell proliferation due to the increase in blood flow and micronutrient delivery. However, it can also be a sign of tumorigenesis, the incidence of which increases with advancing age (Konturek & Barczynski, 2012; Rajabi et al., 2019). This can be interpreted as a positive result, bearing in mind we did not observe an increase in either TSH concentration or the microcirculation of small follicles.

We want to point out both several advantages and the necessity of this type of studies. Though structural parameters need time to change, it is absolutely justified to take into account this level of organization when investigating the effects of aging on an endocrine gland. Namely, both acute and chronic

administration of various treatments (drugs, supplements) has been shown to lead to significant changes in thyroid structure, which is reflected in parenchymal alterations (Giuliani et al., 2014, 2017; Šošić-Jurjević et al., 2014; Miler et al., 2017). Thus, it is of great importance to define and list all the changes in old thyroids, thus far lacking in the literature, to set a clear ground for different experimental designs which would use OA thyroids in their studies. Endocrine signaling is very fast, however, alterations caused by a treatment or just aging can be written into the gland histoarchitecture, particularly on the ultrastructural level. This implies that the structural level is equally important as the functional (molecular) level, and furthermore that structural data may be supported by functional (hormonal, gene, protein expression) results.

In conclusion, we reported that the old-aged thyroid did not preserve the capacity to produce thyroid hormones, since hormone synthesis was observed to a much lesser extent than in YA thyroids (Fig. 10). The gland's synthetic capacity was characterized by lower T_4 production due to the downregulation of iodide import and thyroid gland unresponsiveness to TSH. The latter also caused reduced T_4 secretion, which was observed as a lower T_4 concentration in the serum of OA rats (Fig. 10).

Supplementary material. To view supplementary material for this article, please visit https://doi.org/10.1017/S1431927621000064.

Acknowledgments. This work was supported by the Ministry of Education, Science and Technological Development of the Republic of Serbia, Contract number 451-03-68/2020-14/200007. We are grateful to academician Prof. Dr. Vladimir Bumbaširević, Asst. Prof. Tamara Kravić Stevović, Tamara Martinović, and Darko Ćirić, all from the Institute of Histology and Embriology "Aleksandar Đ. Kostić", School of Medicine, University of Belgrade, for their valuable help in the ultrastructural analysis. We are grateful to Mrs. Maja Vojvodić, an English language professional, for her help in proofreading the manuscript.

References

Ajdžanović V, Miler M, Živanović J, Filipović B, Šošić-Jurjević B, Popovska-Perčinić F & Milošević V (2020). The adrenal cortex after estradiol or daidzein application in a rat model of the andropause: Structural and hormonal study. *Ann Anat* **230**, 151487.

Ajdžanović VZ, Jarić IM, Živanović JB, Filipović BR, Šošić-Jurjević BT, Ristić NM, Stanković SD & Milošević VL (2016). Histological parameters of the adrenal cortex after testosterone application in a rat model of the andropause. *Histol Histopathol* **31**, 1209–1220.

Ajdžanović VZ, Trifunović S, Miljić D, Šošić-Jurjević B, Filipović B, Miler M, Ristić N, Manojlović-Stojanoski M & Milošević V (2018). Somatopause, weaknesses of the therapeutic approaches and the cautious optimism based on experimental ageing studies with soy isoflavones. *EXCLI J* **17**, 279–301.

Armengol MP, Juan M, Lucas-Martín A, Fernández-Figueras MT, Jaraquemada D, Gallart T & Pujol-Borrell R (2001). Thyroid autoimmune disease. *Am J Pathol* **159**, 861–873.

Barbesino G (2019). Thyroid function changes in the elderly and their relationship to cardiovascular health: A mini-review. *Gerontology* **65**, 1–8.

Bizhanova A & Kopp P (2009). The sodium-iodide symporter NIS and pendrin in iodide homeostasis of the thyroid. *Endocrinology* **150**, 1084–1090.

Chahal H & Drake W (2007). The endocrine system and ageing. *J Pathol* **211**, 173–180.

Chen C-R, Hamidi S, Braley-Mullen H, Nagayama Y, Bresee C, Aliesky HA, Rapoport B & McLachlan SM (2010). Antibodies to thyroid peroxidase arise spontaneously with Age in NOD.H-2h4 mice and appear after thyroglobulin antibodies. *Endocrinology* **151**, 4583–4593.

Corrêa Da Costa VM, Moreira DG & Rosenthal D (2001). Thyroid function and aging: Gender-related differences. *J Endocrinol* **171**, 193–198.

Donda A & Lemarchand-Beraud T (1989). Aging alters the activity of 5′-deiodinase in the adenohypophysis, thyroid gland, and liver of the male rat. *Endocrinology* **124**, 1305–1309.

Dorph-Petersen K-A, Nyengaard JR & Gundersen HJG (2001). Tissue shrinkage and unbiased stereological estimation of particle number and size. *J Microsc* **204**, 232–246.

Dunn JT & Dunn AD (2001). Update on intrathyroidal iodine metabolism. *Thyroid* **11**, 407–414.

Faggiano A, Coulot J, Bellon N, Talbot M, Caillou B, Ricard M, Bidart J-M & Schlumberger M (2004). Age-dependent variation of follicular size and expression of iodine transporters in human thyroid tissue. *J Nucl Med* **45**, 232–237.

Fayadat L, Niccoli-Sire P, Lanet J & Franc JL (1998). Human thyroperoxidase Is largely retained and rapidly degraded in the endoplasmic reticulum. Its *N*-glycans are required for folding and intracellular trafficking. *Endocrinology* **139**, 4277–4285.

Giuliani C, Bucci I, Di Santo S, Rossi C, Grassadonia A, Piantelli M, Monaco F & Napolitano G (2014). The flavonoid quercetin inhibits thyroid-restricted genes expression and thyroid function. *Food Chem Toxicol* **66**, 23–29.

Giuliani C, Iezzi M, Ciolli L, Hysi A, Bucci I, Di Santo S, Rossi C, Zucchelli M & Napolitano G (2017). Resveratrol has anti-thyroid effects both in vitro and in vivo. *Food Chem Toxicol* **107**, 237–247.

Gundersen HJ & Jensen EB (1987). The efficiency of systematic sampling in stereology and its prediction. *J Microsc* **147**, 229–263.

Konturek A & Barczynski M (2012. Vascular endothelial growth factor (VEGF) and epidermal growth factor (EGF) in papillary thyroid cancer. In *Thyroid and Parathyroid Diseases - New Insights Into Some Old and Some New Issues*, Ward LS (Ed.), pp. 87–94. Rijeka, Croatia: InTech.

Kotani T & Ohtaki S (1987). Characterization of thyroid follicular cell apical plasma membrane peroxidase using monoclonal antibody. *Endocrinol Jpn* **34**, 407–413.

Lee J, Yi S, Kang YE, Kim H-W, Joung KH, Sul HJ, Kim KS & Shong M (2016). Morphological and functional changes in the thyroid follicles of the aged murine and humans. *J Pathol Transl Med* **50**, 426–435.

Mariotti S, Franceschi C, Cossarizza A & Pinchera N (1995). The aging thyroid. *Endocr Rev* **16**, 686–715.

Martin-Lacave I, Conde E, Montero C & Galera-Davidson H (1992). Quantitative changes in the frequency and distribution of the C-cell population in the rat thyroid gland with age. *Cell Tissue Res* **270**, 73–77.

Miler M, Jarić I, Živanović J, Ajdžanović V, Tanić N, Milošević V & Šošić-Jurjević B (2017). Citrus flavanones mildly interfere with pituitary-thyroid axis in old-aged male rats. *Acta Histochem* **119**, 292–301.

Miler M, Šošić-Jurjević B, Nestorović N, Ristić N, Medigović I, Savin S, Milošević V, Šošič-Jurjević B, Nestorović N, Ristić N, Medigović I, Savin S & Milošević V (2014). Morphological and functional changes in pituitary-thyroid axis following prolonged exposure of female rats to constant light. *J Morphol* **275**, 1161–1172.

Miler M, Živanović J, Ajdžanović V, Milenkovic D, Jarić I, Šošić-Jurjević B & Milošević V (2020). Citrus flavanones upregulate thyrotroph Sirt1 and differently affect thyroid Nrf2 expressions in old-aged Wistar rats. *J Agric Food Chem* **68**, 8242–8254.

Moreira DG, Marassi MP, Corrêa da Costa VM, Carvalho DP & Rosenthal D (2005). Effects of ageing and pharmacological hypothyroidism on pituitary-thyroid axis of Dutch-Miranda and Wistar rats. *Exp Gerontol* **40**, 330–334.

Rajabi S, Dehghan MH, Dastmalchi R, Mashayekhi FJ, Salami S & Hedayati M (2019). The roles and role-players in thyroid cancer angiogenesis. *Endocr J* **66**, 277–293.

Rao-Rupanagudi S, Heywood R & Gopinath C (1992). Age-related changes in thyroid structure and function in Sprague-Dawley rats. *Vet Pathol* **29**, 278–287.

Silvestri E, Lombardi A, de Lange P, Schiavo L, Lanni A, Goglia F, Visser TJ & Moreno M (2008). Age-related changes in renal and hepatic cellular mechanisms associated with variations in rat serum thyroid hormone levels. *Am J Physiol-Endoc M* **294**, E1160–E1168.

Song Y, Driessens N, Costa M, De Deken X, Detours V, Corvilain B, Maenhaut C, Miot F, Van Sande J, Many M-C & Dumont JE (2007).

Roles of hydrogen peroxide in thyroid physiology and disease. *J Clin Endocrinol Metab* **92**, 3764–3773.

Šošić-Jurjević B, Filipović B, Renko K, Miler M, Trifunović S, Ajdžanovič V, Köhrle J & Milošević V (2015). Testosterone and estradiol treatments differently affect pituitary-thyroid axis and liver deiodinase 1 activity in orchidectomized middle-aged rats. *Exp Gerontol* **72**, 85–98.

Šošić-Jurjević B, Filipović B, Wirth EK, Živanović J, Radulović N, Janković S, Milošević V & Köhrle J (2014). Soy isoflavones interfere with thyroid hormone homeostasis in orchidectomized middle-aged rats. *Toxicol Appl Pharmacol* **278**, 124–134.

Uchiyama Y, Murakami G & Igarashi M (1986). Changes in colloid droplets and dense bodies in rat thyroid follicular cells during 24 hours: Fine structural and morphometric studies. *Am J Anat* **175**, 15–22.

Wang T, Liang X, Abeysekera IR, Iqbal U, Duan Q, Naha G, Lin L & Yao X (2017). Activation of the Nrf2-keap 1 pathway in short-term iodide excess in thyroid in rats. *Oxid Med Cell Longevity* **2017**, Article ID 4383652.

Živanović J, Jarić I, Ajdžanović V, Mojić M, Miler M, Šošić-Jurjević B, Milošević V & Filipović B (2019). Daidzein upregulates anti-aging protein klotho and NaPi 2a cotransporter in a rat model of the andropause. *Ann Anat* **221**, 27–37.